

The case of a southern European glacier ~~that~~which survived Roman and Medieval warm periods but is disappearing under recent warming

Ana Moreno¹, Miguel Bartolomé², Juan Ignacio López-Moreno¹, Jorge Pey^{1,3}, Juan Pablo Corella⁴, Jordi García-Orellana^{5,6}, Carlos Sancho⁷, María Leunda^{7,8}, Graciela Gil-Romera^{9,1}, Penélope González-Sampériz¹, Carlos Pérez-Mejías¹⁰, Francisco Navarro¹¹, Jaime Otero-García¹¹, Javier Lapazaran¹¹, Esteban Alonso-González¹, Cristina Cid¹², Jerónimo López-Martínez¹³, Belén Oliva-Urcia¹³, Sérgio Henrique Faria^{14,15}, María José Sierra⁴, Rocío Millán⁴, Xavier Querol¹⁶, Andrés Alastuey¹⁶ and José M. García-Ruiz¹

1. Departamento de Procesos Geoambientales y Cambio Global, Instituto Pirenaico de Ecología – CSIC, Zaragoza, Spain
2. Departamento de Geología, Museo de Ciencias Naturales - CSIC, Madrid, Spain
3. Fundación Aragonesa para la Investigación y el Desarrollo, ARAID, Zaragoza, Spain
4. CIEMAT — Environmental Department (DMA), Avenida Complutense 40, Madrid, Spain
5. Institut de Ciència i Tecnologia Ambientals, Universitat Autònoma de Barcelona, Barcelona, Spain
6. Departament de Física, Universitat Autònoma de Barcelona, Barcelona, Spain
7. Institute of Plant Sciences & Oeschger Centre for Climate Change Research, Bern, Switzerland
8. Swiss Federal Research Institute for Forest, Snow and Landscape Research WSL, Birmensdorf, Switzerland
9. Department of Ecology, Faculty of Biology, Philipps-Marburg University, Marburg, Germany
10. Institute of Global Environmental Change, Xi'an Jiaotong University, Xi'an, China
11. Departamento de Matemática Aplicada a las TIC, ETSI de Telecomunicación, Universidad Politécnica de Madrid, Madrid, Spain
12. Centro de Astrobiología – CSIC-INTA, Madrid, Spain
13. Departamento de Geología y Geoquímica, Facultad de Ciencias, Universidad Autónoma de Madrid, Madrid, Spain
14. Basque Centre for Climate Change (BC3), Leioa, Spain
15. IKERBASQUE, Basque Foundation for Science, Bilbao, Spain
16. Institute of Environmental Assessment and Water Research – CSIC, Barcelona, Spain

† Deceased

Corresponding author: Ana Moreno (amoreno@ipe.csic.es) ORCID: 0000-0001-7357-584X

Keywords

Pyrenees, mountain glacier, current global warming, Medieval Climate Anomaly, Monte Perdido

Código de campo cambiado

Abstract

Mountain glaciers have generally experienced an accelerated retreat over the last three decades as a rapid response to current global warming. However, the response to previous warm periods in the Holocene is not well-described for glaciers of the southern Europe mountain ranges, such as the Pyrenees. The situation during the Medieval Climate Anomaly (900-1300 CE) is particularly relevant since it is not certain whether the southern European glaciers just experienced significant ice loss or whether they actually disappeared. We present here the first chronological study of a glacier located in the Central Pyrenees (NE Spain), the Monte Perdido Glacier (MPG), carried out by different radiochronological techniques and a comparison with geochemical proxies from neighboring paleoclimate records. The chronological model evidences that the glacier ~~endured~~ persisted during the Roman Period and the Medieval Climate Anomaly. The ~~lack apparent absence~~ of ice ~~record dated~~ from the ~~last past~~ ~600 years suggests that ~~any~~ the ice ~~formed accumulated~~ during the Little Ice Age has ~~melted since ablated away~~. This interpretation is supported by measured concentrations of anthropogenic metals, including Zn, Se, Cd, Hg and Pb, which have concentrations well below those typical of industrial-age ice measured at other glaciers in Europe. This study strengthens the general understanding that warming of the past few decades has been exceptional for the past two millennia~~The analyses of several metals with anthropogenic source that characterize the Industrial Period, such as Zn, Se, Cd, Hg and Pb, reveal low concentrations in MPG ice, which provides further evidence about the absence of the most recent ice. This study confirms the exceptional warming of the last decades in the context of the last two millennia.~~

1. Introduction

Mountain glaciers are sensitive to climate variations on temporal scales from decades to centuries. It is well known that summer temperature and winter precipitation are the most important climate parameters influencing glacier mass balance (Oerlemans, 2001). Therefore, continuous records of past glacier size fluctuations provide valuable information about the timing and magnitude of Holocene climate shifts, which contributed to explain the characteristics and evolution of plant cover, human movements and land use (Solomina et al., 2015, 2016). Several glacier advances during the Neoglacial (which started around 6000-5000 years ago) have been identified (Bohleber et al., 2020) and associated to sustained cooling periods across the North Atlantic (Wanner et al., 2011). The most recent period of global glacier expansion took place during the Little Ice Age (LIA), beginning in the 13th century and reaching a maximum between the 17th and 19th centuries (Solomina et al., 2016). Afterwards, most glaciers worldwide have retreated rapidly, as indicated by measurements of [changes in](#) ice volume and ice-covered area, and this trend seems to have accelerated over the last three decades (Marzeion et al., 2014; Zemp et al., 2015, 2019).

Despite broad agreement on millennial-scale trends in global glacier fluctuations and Holocene climate variability (Davis et al., 2009; Solomina et al., 2015), regional variations are not so well constrained. The Pyrenees ~~is~~[are](#) a mountain range that currently hosts the majority of the southernmost glaciers in Europe. In this mountain chain there is a significant lack of knowledge about Holocene glacier fluctuations, with ~~few-little~~[evidences](#) of Neoglacial advances (García-Ruiz et al., 2020). Based on Pyrenean tree-ring chronologies, summer temperatures during the Medieval Climate Anomaly (MCA, circa 900–1300 CE) were estimated to have been as warm as those of the 20th century (Büntgen et al., 2017), but no information is available on the glacier response to MCA warming. Conversely, glacier advance during the LIA is well constrained in the Pyrenees (García-Ruiz et al., 2014; González Trueba et al., 2008; Hughes, 2018; Oliva et al., 2018) and ~~a~~[a](#) significant deglaciation is also evident in recent times (López-Moreno et al., 2016; Rico et al., 2017). In particular, the period from the 1980s to present has been the most intense in terms of the number of glaciers that disappeared (from 39 inventoried Pyrenean glaciers in 1984 to 19 at present; Rico et

Con formato: Inglés (Estados Unidos)

al. 2017). Given the small size of the Pyrenean glaciers and their current critical situation in the context of global warming, we hypothesize that they could have disappeared completely during warm periods such as the MCA.

This study is focused on Monte Perdido Glacier (MPG), located in the Marboré Cirque in the Spanish Central Pyrenees. MPG is currently one of the ~~best-most~~ most intensely monitored small glaciers ($<0.5 \text{ km}^2$) worldwide (López-Moreno et al., 2016, 2019). Previous research based on different ground-based remote sensing techniques has demonstrated a rapid retreat of this glacier, with an average loss of ice thickness of about one meter per year since 1981 (López-Moreno et al., 2016, 2019). This glacier is located in one of the few valleys in the Pyrenees where information about Holocene glacier fluctuations exists. The outermost moraine in Marboré Cirque was recently dated at $6900 \pm 800 \text{ }^{36}\text{Cl yr BP}$ (García-Ruiz et al., 2020), which is the oldest Holocene date available for glacial deposits in Spain, and indicates a glacier advance during the Neoglacial period. Other minor advances would have occurred in MPG prior to the LIA, as inferred from three polished surfaces dated at 3500 ± 400 , 2500 ± 300 and $1100 \pm 100 \text{ }^{36}\text{Cl yr BP}$ (García-Ruiz et al., 2020). Unfortunately, no information has been obtained on the glacier response to Roman or MCA warming periods, remaining an open question whether MPG just experienced significant ice loss or melted away totally. Most likely, the voluminous moraine at the foot of the Monte Perdido Massif was deposited during the LIA, indicating an important glacier advance. These results, together with ~~the~~ evidences of long-term retreat from its LIA position indicated by pictures and moraines, ~~suggested~~ that this glacier could disappear over the next few decades (López-Moreno et al., 2016).

The present study aims to reconstruct the chronology of MPG ice sequence by using a variety of dating techniques and the analysis of several proxies associated ~~to~~ with environmental and anthropogenic changes measured on a set of samples taken from a transect. Such analyses will fill the existing knowledge gaps and ~~answer~~ address the key question of whether Pyrenean glaciers may have survived previous Holocene warm periods.

2. Study area

The MPG (42°40'50"N; 0°02'15"E) is located in the Central Spanish Pyrenees, in the Ordesa and Monte Perdido National Park (OMPNP) (Fig. 1). It currently consists of two separate ice bodies, which were connected in the past. Both are north facing, lie on structural flats beneath the main summit of the Monte Perdido Peak (3355 m a.s.l.) and are surrounded by nearly vertical cliffs of 500–800 m in height under conditions of mountain permafrost (Serrano et al., 2020). At the base of the cliffs, the Cinca River flows directly from the glacier and the surrounding slopes, and has created a longitudinal west–east basin called the Marboré Cirque (5.8 km²). This is the area within the Pyrenees with the highest variety of recent morainic deposits (García-Ruiz et al., 2014, 2020). Additionally, a 6 m thick sediment core obtained in 2011 from a lake inside the cirque (Marboré Lake) provided valuable information from the last 14,600 years of the depositional evolution of the lake (Oliva-Urcia et al., 2018) and of the regional variations in vegetation cover (Leunda et al., 2017). The Marboré Lake (2595 m a.s.l.) is located in the Marboré or Tucarroya Cirque, in the northern face at the foot of the Monte Perdido massif. The distance between the lake and the MPG is approximately 1300 m and, therefore, both have been affected by similar palaeoenvironmental conditions past climate changes.

The total surface area of MPG in 2016 was 0.385 km², with an average decrease in glacier ice thickness of 6.1 m during over the period 2011 - 2017 (López-Moreno et al., 2019). According to recent measurements of air temperature (July 2014 to October 2017), the 0 °C isotherm lies at 2945 m a.s.l., suggesting that the potential glacier accumulation area is very small, even-inexistent and perhaps non-existent, during warm years. The average summer (June to September) temperature at the foot of the glacier from 2014 to 2017 has been was of 7.3 °C (López-Moreno et al., 2019). No direct observations of precipitation are available at-from the glacier location, but the maximum accumulated snow by late April in the three available years (2014, 2015 and 2017, when no scanning limitations occurred and-when the whole glacier was scanned) was 3.23 m, and field-measured average snow density was 454 kg m⁻³, indicating that the total water equivalent during the main accumulation period (October to April) could be equivalent to 1500 mm has recently been about 1.5 m (López-Moreno et al., 2019).

3. Material and methods

3.1. Ice sampling and storage

Ice sampling on MPG was carried out in September 2017 along a chrono-stratigraphical sequence ~~covering~~ from the lowermost and assumedly oldest to the uppermost and assumedly youngest ice preserved in the glacier, following the isochronal layers that emerge in the ablation zone (Fig. 2A). ~~Unfortunately, the extraction of v~~Vertical cores ~~was not possible~~were not recovered because the glacier does not ~~currently~~ meet ~~any of~~ the usual glacio-meteorological and topographical criteria required to obtain a preserved ice-core stratigraphy. The unfulfilled criteria include low temperatures to prevent water percolation or a large extension and flat surface topography to minimize the influence of glacier flow (Garzonio et al., 2018). Samples were collected in an area with no evidence of major current ice movement ~~(or very low)~~, as confirmed by results from interferometric radar and GNSS measurements (López-Moreno et al., 2019). Due to the small size of this glacier and the absence of ice movement, we expected the ice to be frozen to the permafrost bedrock, and hence nearly stagnant, ~~to become of~~thereby reaching a substantial age, as indicated by previous studies in similar glaciers (Gabrielli et al., 2016; Haeberli et al., 2004). The sampling sector lies in the ablation zone of the present-day MPG and has been eroded to form a current steady slope of 20° where it is possible to observe the primary stratigraphy, marked by clear debris-rich layers. The distribution of these debris-rich layers is rather regular and extends laterally (Fig. 2B), as would be expected for the primary stratification resulting from the original surface deposition ~~at surface~~ of snow and debris. Therefore, these layers are considered isochrones, and confirm and facilitate the sampling along the slope, from the oldest to the ~~newest~~youngest ice preserved in the glacier.

We measured one-meter thickness using a Jacob's staff at each sampling point along the slope (inset in Fig. 2B2A). The tilt of the ice layers was unclear but, since previous studies calculated about 30 m of ice thickness (López-Moreno et al., 2019), the ice layers ~~are~~ probably dip steeply, quite tilted downward as ~~detailed~~illustrated in Fig. 2A. After removing ~0.5 m of (possibly contaminated) surface ice, three or four horizontal

183 ~~cores, each of diameter 6 cm and length 25 cm, were sampled using a~~ Once cleaned the
184 ~~most superficial ice (ca. 50 cm) to avoid possible ice formed recently, we recovered at~~
185 ~~every sampling position 3–4 small horizontal cores (6 cm in diameter and 25 cm in~~
186 ~~length) using a~~ custom stainless-steel crown adaptor on a cordless power drill (Fig. 2C).
187 Following this sampling procedure we recovered a total of 100 samples. The ice
188 samples were stored in a freezer room at the IPE-CSIC in Zaragoza until they were
189 melted and analysed to obtain their chronology combining ^{210}Pb , ^{137}Cs and ^{14}C
190 techniques, and their geochemical composition in trace metals, such as Pb or Hg (see
191 below).

192 3.2. Dating by ~~using~~ ^{210}Pb and ^{137}Cs .

193 The isotope ^{137}Cs , ~~usually~~ associated to the fallout from nuclear tests during the 1950s
194 and the 1960s, as well as the Chernobyl (1986) (Haeberli et al., 1988) and Fukushima
195 (2011) ~~nuclear~~ accidents, was investigated by γ -spectrometry in five samples recovered
196 towards the top of the MPG chronological sequence (MP-61, MP-82, MP-97, MP-98,
197 MP-100, Table 1). In addition, ten samples were selected to perform a ^{210}Pb analysis as
198 an independent dating method to obtain the age model of approximately the last
199 hundred years of glacier ice (Eichler et al., 2000; Herren et al., 2013). These samples
200 were selected also from the top of the ice sequence to collect the younger ice (Table
201 2). Determination of ^{210}Pb activities was accomplished through the measurement of its
202 daughter nuclide, ^{210}Po , by α -spectrometry following the methodology described in
203 (Sanchez-Cabeza et al., 1998) (Table 2).

204 3.3. Dating by ^{14}C method.

205 Sixteen accelerator mass spectrometry (AMS) ^{14}C dates from MPG ice were obtained
206 by combining bulk organic matter (9 samples), pollen concentrates (3 samples), bulk
207 sediment accumulated in filters (2 filters), and water-insoluble organic carbon (WIOC)
208 particles (2 samples) (Table 3). The procedure to select these samples was as follows:

209 (i) Using a binocular microscope [x10], we picked up organic particles for dating from
210 selected ice samples. However, the small size of the handpicked organic remains
211 prevented us from classifying them. As a result, we obtained 9 samples (MP-1, MP-42,

Con formato: Inglés (Estados Unidos)

MP-48, MP-67, MP-68, MP-69, MP-70, MP-73, MP-100, Table 3) that were sent to the Direct AMS laboratory (Seattle, USA) for dating. The selection of those nine samples was based on the amount of debris found in the sample, once the ice was melted.

(ii) Pollen concentrates were prepared from three samples (MP-30, MP-70 and MP-100) to complete the previous set with the aim of replicating some of the results (MP-70 and MP-100) and obtaining new dates (MP-30). Preparation followed the standard palynological method, including a chemical treatment and mineral separation in heavy liquid (Thoulet: density 2.0; Moore et al., 1991). The effects of meltwater percolation on pollen in snow, firn and glacial ice are not fully understood and currently challenge the use of pollen in ice-core studies (Ewing et al., 2014). Just in few cases pollen has appeared as a potential dating material, when seasonal layers are preserved (Festi et al., 2017). Yet, pollen concentrates have been used in other type of archives with high success (Fletcher et al., 2017), opening the door to apply the same methodology here.

(iii) Two ice samples (MP-67 and MP-81), which appeared darker than others once melted, were filtered throughout a filtration line connected to a vacuum pump using ~~47-mm~~ quartz fiber filters (PALL tissuquartz 2500QAT-UP), parameterized at controlled conditions (temperature: 22 – 24 °C; relative humidity 25 – 35 %) and weighted twice in different days. Abundant material was obtained, but no control was made on the composition and amount of organic material versus other types of input. The three concentrated pollen samples and the two filters were dated at the same ¹⁴C dating laboratory (Direct AMS, Seattle, USA) (Table 3).

(iv) Finally, two more samples were dated at the Laboratory of Environmental Chemistry, Paul Scherrer Institute (Switzerland) removing the outer part of the ice core segment for decontamination purposes (Jenk et al., 2009). Since organic fragments (plants, wood, insects) are rarely found in mountain glaciers, a ~~new~~, complementary dating tool was recently developed based on extracting the microgram-amounts of the water-insoluble organic carbon (WIOC) fraction of carbonaceous aerosols embedded in the ice matrix for subsequent ¹⁴C dating (Uglietti et al., 2016). These two samples, labelled as MP10m and MP59m at the WIOC facility (Table 3), were selected as they were the only ones with sufficient ice volume available.

242 Once the 16 radiocarbon ages were obtained, we converted them into calendar ages
243 by using the CALIB 5.0.2 software, which uses the most updated dataset, INTCAL13
244 (Reimer et al., 2013) (Table 3). The median of the one- σ probability interval was
245 selected for these dates, resulting in highly variable errors in the calendar ages
246 obtained (from 30 years on the bulk organic samples to more than 200 years on pollen
247 and WIOC samples). While the first method to select organic remains at the
248 microscope resulted the best option, the pollen concentration and filtering methods
249 used to isolate organic matter to be dated by ^{14}C were, unfortunately, not successful.
250 Finally, from the initial 16 dates, we had to discard seven according to the following
251 criteria (see the “comments” column in Table 3):

- 252 - Sample MP-46 (D-AMS 025295) was the only one discarded from the nine initial
253 bulk organic matter samples. We suspect that the very recent age obtained
254 (1897 ± 20 CE, Table 3) is due to the sample contamination, since small plastic
255 debris coming off from the painting used in the coring device were identified
256 under the microscope.
- 257 - From the two WIOC-dated samples, one was discarded (MP10m) due to the
258 low carbon content ($5.3 \mu\text{g}$), thus providing too inaccurate results (854 ± 721
259 CE, with an unacceptable large uncertainty). The other sample (MP59m), with
260 higher organic carbon content ($28.7 \mu\text{g}$), was incorporated into the age model
261 in spite of its error above 200 yr (1046 ± 242 CE).
- 262 - The three pollen concentrates provided unreliably old dates with very high
263 errors, likely due to the small amount of pollen that we were able to
264 concentrate (errors above 200 yr, Table 3). Obtaining old dates from pollen is a
265 quite common problem not yet solved in the literature (Kilian et al., 2002).
- 266 - Similarly, we discarded the two filter samples MP-67 and MP-81 (D-AMS
267 029894 and D-AMS 033972, respectively). The material accumulated in the
268 filters was a mixture of particles containing detrital carbonate eroded from
269 Eocene limestones or supplied by Saharan dust, which was not removed and
270 probably influenced the results incorporating allochthonous carbon to the
271 samples.

Finally, nine dates were employed to infer the chronology of the MPG sequence. The depth–age model was created using a linear regression in the R package CLAM 2.2 (Blaauw, 2010; Blaauw et al., 2019).

3.4. Trace elements in soluble and insoluble material.

~~35–Thirty-five~~ selected ice samples from the altitudinal transect were melted and filtered through a filtration ramp connected to a vacuum pump using ~~47 mm~~ quartz fibre filters (PALL tissuquartz 2500QAT-UP). Filters were pre-heated at 250 °C and thereafter prepared in controlled conditions (temperature: 22 – 24 °C; relative humidity: 25 – 35 %) before and after filtration. Subsequently, they were weighted in two different days. Mass difference between blank and sampled filters was used to calculate the amount of insoluble material entrapped in ice samples. For every sample, an aliquot and a filter were obtained. From aliquots, anions and cations, as well as major and trace elements were determined. From filters, we determined major and trace elements, as well as organic and elemental carbon, following the method devised by Pey et al. (2013) (Table 4). Basically, an acidic digestion (HNO₃:HF:HClO₄) of half of each filter was conducted, driven to complete dryness, being the remaining material re-dissolved in HNO₃. Inductively coupled plasma mass spectrometry (ICP-MS) and inductively coupled plasma atomic emission spectroscopy (ICP-AES) were used to determine major and trace elements, respectively. From the other half of each filter, a 1.5 cm² section was used to determine Organic Carbon (OC) and Elemental Carbon (EC) concentrations by using a SUNSET thermo-optical analyzer, following the EUSAAR_2 temperature protocol. Table 1 also contains the Enrichment Factors (EFs), calculated as follows:

$$EF_{iCDD} = \frac{X_{iCDD}/Al_{CDD}}{X_{iUC}/Al_{UC}} ; EF_{iMPGID} = \frac{X_{iMPGID}/Al_{MPGID}}{X_{iUC}/Al_{UC}} ; EF_i = \frac{X_{iCDD}/Al_{CDD}}{X_{iMPGID}/Al_{MPGID}}$$

where EF_{iCDD} is the Al-normalised Enrichment Factor with respect to the Upper Crust (UC, Taylor and McLennan, 1995) of an ‘i’ element in the current Ordesa’s deposited dust (CDD); EF_{iMPGID} is the Al-normalised Enrichment Factor with respect to the UC of

an 'i' element in the current MPG ice dust (*MPGID*); and EF_i is the Al-normalised Enrichment Factor with respect to *CODD* of an 'i' element in the *MPGID*.

Regarding the Pb/Al ratio, we carried out a normalization with Al in both, ice and lake records, to disentangle the anthropogenic lead variability from possible detrital inputs. Aluminium has been selected for normalization since this lithogenic element is immobile and abundant in carbonated watersheds (Corella et al., 2018).

3.5. Hg determination.

Total Hg concentration measurements were carried out in 21 selected samples by Atomic Absorption Spectrophotometry using an Advance Mercury Analyzer (AMA 254, LECO Company). This equipment is specifically designed for direct mercury determination in solid and liquid samples without sample chemical pre-treatment. Certified reference materials were used to determine the accuracy and precision of the Hg measurements. These reference materials were ZC73027 (rice, $4.8 \pm 0.8 \mu\text{g kg}^{-1}$) and CRM051-050 (clay soil, $4.08 \pm 0.09 \text{ mg kg}^{-1}$). The standard deviation (repeatability) was $\leq 15 \%$ and the relative uncertainty associated with the method (with a confidence level of about 95 %) was $\pm 20 \%$. All analyses were run at least three times. Total metal concentrations were expressed in $\mu\text{g g}^{-1}$ of dry weight sediment due to the low amount detected.

4. Results

4.1. Chronological model

To date the ice sequence from MPG we compiled the results from ^{137}Cs , ^{210}Pb and ^{14}C methods. First, ~~it is remarkable we note~~ that the all samples analyzed for ^{137}Cs presented activities below the MDA values (Minimum Detection Activity) extremely low ~~absence of ^{137}Cs activity in the five samples analyzed, all below the MDA values (Minimum Detection Activity)~~ (Table 1). ~~This~~ These values, compared to other ^{137}Cs values in glacier records (e.g. (Di Stefano et al., 2019), indicate ~~implies~~ that all samples are older than 60–65 years and therefore they were not exposed to the atmosphere after 1950 CE. ~~Another possibility that was discarded upon obtaining ^{14}C dates, is that all samples were younger than 1950 CE.~~ Similarly, ^{210}Pb activity was also undetectable

Con formato: Color de fuente:
Automático

Con formato: Color de fuente:
Automático, Superíndice

Con formato: Color de fuente:
Automático

in most cases, except in three samples (MP-100, MP-73 and MP-76) with concentrations above ~~minimum detection activity~~MDA (MDA; Table 2), but well below the usual ^{210}Pb activity concentrations in glacier surface samples from European Alps, which are on average $86 \pm 16 \text{ mBq kg}^{-1}$ (Gäggeler et al., 2020). These three samples contained a large amount of lithogenic particulate material from atmospheric dust or ash deposits, likely causing the observed values. Thus, the absence of ^{210}Pb activity in the analysed samples suggests that MPG ice samples were very likely older than 100 years and the ^{210}Pb had completely decayed. We then built up the proposed MPG chronology using only AMS ^{14}C dating.

Regarding ^{14}C dating, we took most of the ice samples for dating in sections where dark debris layers alternated every ca. 5 m with cleaner and clearer ice (Fig. 2). The debris-rich layers were composed of detrital, silty-sandy size deposits, likely coming from wind-blown particles (e.g. black carbon-rich particles, dust) and from erosive processes of the limestone catchment, including frost weathering and the fall of gravel-sized particles from the surrounding cliffs. These debris-rich layers do not have a subglacially-derived origin since they are observed all along the sample profile and large accumulation of debris-or pinnacles, both-characteristics of subglacially-derived glacier till, were not found in present at MPG. These debris layers contain more organic remains than those formed by clear ice, making them ideal spots to find datable remains.

Interestingly, the frequency of debris layers increases towards the top of the glacier sequence. We consider the accumulation of debris layers to be indicative of reduced ice accumulation and dominance of ablation periods. In such situations, the detrital and organic material concentrates as the ice melts, giving its characteristic dark colour to the ice layers. The major concentration of such layers occurred among samples MP-67 and MP-73 (Table 3), thus suggesting the dominance of ablation processes. Therefore, we run the depth-age model setting a hiatus at 73 m depth, where we ~~think infer~~ an interruption in the ice accumulation was produced. Finally, as explained in the ~~m~~Methods-section, the depth-age-model was constructed with ~~nine 9~~ of the 16 initially dated ~~16~~-samples (Table 3). Given the scattered depths at which dates concentrate, we chose to perform a non-smooth, linear regression for preventing any

model over-fitting and a spurious ~~age~~-depth-~~age~~ relationship (Fig. 3). ~~Full details on~~ how the model was performed and a reproducible workflow with the current chronological dataset ~~are stored~~ are available at <https://zenodo.org/record/3886911>.

Código de campo cambiado

4.2. Trace elements

We have used the averaged concentration values of major and trace elements currently obtained at a monitoring station located at [the Ordesa site](#) (OMPNP; ~8 km away from the MPG, at 1190 m a.s.l.), where deposited atmospheric particulate matter is sampled monthly (Table 4) (Pey et al., 2020). Interestingly, the elements that are abundant nowadays in the Ordesa station are not so frequent in the ice from MPG. Indicators such as organic carbon, Zn, Se and Cd concentrations, all of which are potential proxies of current anthropogenic emissions, are much higher in the samples from Ordesa, which are representative of today's atmosphere, than in the ice samples from the MPG. In fact, similar results appear when comparing with other glaciers in Europe where the EFs for some elements (eg. Zn, Ag, Bi, Sb and Cd) (Gabrieli et al., 2011) are well above the crustal value (Gabrieli et al., 2011), demonstrating the predominance of non-crustal deposits and suggesting an anthropogenic origin. The low concentration of ~~these~~-~~those~~ elements in MPG samples could indicate their disappearance ~~from~~-~~from the~~ glacier surface layers due to ~~its~~-continuous melting. This supports our suggested depth-age model (Fig. 3), in which ages from the Industrial Period are not recorded. Conversely, the Al-normalised enrichment factor (EF) of Ti, Mn, Cr, Co, Ni, Cu and Pb, elements linked to the natural fraction (dust deposition, lithogenic elements) and mining activities (Corella et al., 2018), are more abundant in the MPG ice samples than in the present-day Ordesa aerosols (Table 4). From them, Cu and Pb were markedly enriched (by a factor >_6) in the MPG ice samples compared with the current deposited aerosols in Ordesa station.

Con formato: Inglés (Estados Unidos)

5. Discussion

5.1. Dating Monte Perdido Glacier ice sequence

Dating ~~the~~ ice from non-polar glaciers is challenging and often problematic as annual layer counting is precluded due to periods without net accumulation, and to common

ice deformation caused by glacier flow (Bohleber, 2019; Festi et al., 2017). The low values in ^{137}C and ^{210}Pb activities in MPG samples compared to other European glaciers (Di Stefano et al., 2019; Festi et al., 2020; Gäggeler et al., 2020) do not allow building any chronology for the last 150 years (Tables 1 and 2) and, therefore, we have constrained the depth-age model of MPG ice using nine ^{14}C absolute dating dates from different materials (Table 3), the absence of ^{137}C and ^{210}Pb in surface ice samples (Di Stefano et al., 2019; Gäggeler et al., 2020), and we have also integrated in the chronology the characteristics of the ice stratigraphy, such as the presence of dark debris-rich layers.

The Our MPG depth-age model suggests that the glacier is composed of ice up to ~2000 years old, and that the glacier's subsequent history has involved three main obtained indicates the presence of ice since 2000 years ago and allows distinguishing three main periods for MPG (Fig. 3). Period I was an accumulation period-phase from 0 to 700 CE. Period II represents an ablation-dominated phase from 700 to 1200 CE, which corresponds to the dark-rich layer interval where more dates are concentrated. Period III corresponds to a new accumulation period-phase from 1200 to 1400 CE. This last period agrees well with an increase in cold season (Oct–May) heavy rainfall events during the cold season (Oct–May) in the Southern Central Pyrenees between 1164 – 1414 CE (Corella et al., 2016), which that most likely resulted on-in higher snow accumulation at high elevation areas, leading to a net accumulation in-on the MPG. Finally, no ice formed during, at least, the last 600 years years has been found today in the MPG. This indicates that the LIA ice has been melted away, pointing to a an-intense ablation-period of intense mass loss since 1850 CE. The MPG age model is supported by, first, a quantitative comparison with present-day atmospheric particulate matter (Table 4) and, second, by the comparison with the paleoenvironmental sequence of the Marboré Lake for the last 2000 years (Corella et al., 2021; Oliva-Urcia et al., 2018) (Fig. 4).

Present-day aerosols in the studied region are well-recorded in-at the nearby Ordesa site (Pey et al., 2020). Following previous studies on present-day atmospheric particulate matter composition from natural, urban or industrial areas (Querol et al., 2007), the values of some elemental ratios (e.g., Cu/Mn, As/Se, Pb/Zn) help to

determine the origin of the particulate matter accumulated today. The Ordesa site can accordingly be mostly defined as remote in terms of atmospheric deposition (“rural background”) while the average composition of MPG ice samples could be defined as a site under the influence of Cu mining and smelting activities, due to the high values of the Cu/Mn, As/Se and Pb/Zn ratios. It is noteworthy that Cu, Ag, and Pb mining and smelting have been historically documented in Bielsa valley during pre-industrial times (Callén, 1996). Indeed, MPG is only 7 km east from some of the largest lead and silver ore deposits in the Central Pyrenees (historical mines of Parzán). The impact of ancient environmental pollution in high alpine environments is archived in the lacustrine sequence of the neighbouring Marboré Lake, providing first evidences of long-range transport of trace metals from historical metal mining and smelting activities during the Roman Period (RP) (Corella et al., 2018, 2021). Similar ice core records from the Alps have also demonstrated the suitability of glacier ice to record local and regional mining and smelting activities during RP and pre-Roman times (More et al., 2017; Preunkert et al., 2019). Even if the enrichment of trace elements in [the](#) MPG ice record may correspond to mining activities during ancient times, the ~~different altitudedistinct~~ [elevation](#) of MPG ~~glacier~~ with respect to ~~records from~~ Alpine glaciers where such activities were recorded (> 4000m a.s.l.), together with the likely processes of redistribution of chemical impurities due to percolation (Pohjola et al., 2002), prevents a firm interpretation of the origin of these elements.

On the other hand, the comparison of Pb/Al ratios from the independently dated records of Marboré Lake and MPG provides further support ~~to the obtained glacier for~~ [our MPG](#) chronology (Fig. 4). In particular, the lack of a Pb/Al peak characterizing the Industrial Period in the upper sequence of the MPG [record, where several samples were analysed \(see ID in Table 5\)](#) ~~confirms-supports~~ the absence of [records from](#) the last two centuries in ~~the MPG ice record~~, in agreement with the [results of](#) ²¹⁰Pb and ¹³⁷Cs analyses. Similarly, the Hg concentration in the glacier is ~~very stableuniform~~ [throughout the ice sequence \(Fig.4\)](#). ~~Hg-eC~~ [Concentrations- of Hg](#) in other ice core records show an increase during the onset of Industrialization at 1800 CE with maximum values typically 3–10 times higher than preindustrial values (Cooke et al., 2020). In [the](#) Marboré Lake, the Hg increase occurred over the last 500 years

450 associated to the maximum activity in the Spanish Almadén mines during the Colonial
451 Period (Corella et al., 2021). Again, these results, lacking an expected increase in Hg
452 levels, support the [depth](#)-age model ~~from~~[for](#) the MPG record where the last six
453 centuries of ice deposition are missing.

454 5.2. Evolution of the Monte Perdido glacier over the last 2000 years

455 The ~~analyzed~~[analysed](#) ice from MPG provides valuable information about the
456 evolution of the glacier ~~during~~[over](#) the last two millennia, which deserves
457 consideration in the regional context. Based on published results, the oldest
458 paleoclimatic information in the Marboré Cirque comes from the Marboré Lake, since
459 no glacier deposits corresponding to the Late Pleistocene have been found in the
460 cirque (García-Ruiz et al., 2014). There is sedimentological evidence that the Marboré
461 Lake was already ice-free at least since the onset of the Bølling period (Greenland
462 Interstadial-1, ~~14,600–12,900~~ yr BP), when clastic sediments were deposited in the
463 lake basin (Leunda et al., 2017; Oliva-Urcia et al., 2018). This is coherent with the
464 nearby La Larri ~~juxta-glacial~~[glaciolacustrine](#) sequence which showed that the main
465 Pineta ~~glacier~~[Glacier](#) had already retreated further up in the headwater by 11 kyr BP
466 (Salazar et al., 2013). In fact, glaciological studies performed in the Central Pyrenees
467 confirm the sudden retreat of glaciers during the Bølling period, when they were
468 reduced to small ice tongues or cirque glaciers (Palacios et al., 2017). The next piece of
469 information comes from the outermost moraine that was dated at 6900 ± 800 ^{36}Cl yr
470 BP (García-Ruiz et al., 2020), corresponding to the Neoglacial advance, a cold period
471 identified in the sediments of ~~Marbore~~[Marboré](#) Lake (Leunda et al., 2017). Other
472 minor advances would have occurred in [the](#) MPG prior to the LIA, as inferred from
473 three polished surfaces dated at 3500 ± 400 , 2500 ± 300 and 1100 ± 100 ^{36}Cl yr BP
474 (García-Ruiz et al., 2020).

475 With the new chronology of the MPG record, we can ascertain that [the](#) MPG has
476 persisted at least since the RP (ca. 2000 years ago). At that time, which is a well-known
477 warm period in the Iberian Peninsula as recorded in both continental (Martín-Puertas
478 et al., 2010; Morellón et al., 2009) and marine sequences (Cisneros et al., 2016;
479 Margaritelli et al., 2020), the glacier was still present, but probably smaller than during

previous Neoglacial times (Figs. 5A and 5B). This situation probably continued during the following cold period, the Dark Ages (DA, Fig 5C) when the glacier advanced as indicated by the polished surface dated at 1100 ± 100 ^{36}Cl yr BP (García-Ruiz et al., 2020). In the Alps, reconstructions based on dating trees found within and at the edge of glacier forefields have revealed a minimum glacier extent during the Iron Age and the RP (Holzhauser et al., 2005), when glaciers were estimated to be smaller than during the 1920s (Ivy-Ochs et al., 2009). Afterwards, in the late RP and the early Middle Ages numerous glaciers in the Alps advanced during the DA, also known as the Göschener II oscillation (Holzhauser et al., 2005).

The [Medieval Climate Anomaly](#) (MCA, 900–1300 CE) is the most recent preindustrial warm era in Europe (Mann et al., 2009). For instance, in the Alps, a general glacier retreat has been observed during this period, mainly associated with a decline in precipitation (Holzhauser et al., 2005). According to the [age-depth-age](#) model, the MPG experienced a ~~spectacular-dramatic retreat-retreat during that period~~ (Fig. 5D), including the complete melting of some minor glaciers in the Marboré Cirque (García-Ruiz et al., 2020). Nevertheless, during the MCA part of MPG was preserved, as we find ice from 0 to 700 CE. No doubt the ice loss was significant, as evidenced by the accumulation of dark strata over a long time interval (600 – 1200 CE) [and the just six meters of ice remaining from that period \(blue horizontal line, Fig.3\)](#). On this basis, we propose that the MPG was dominated by ablation processes during the MCA, ~~leading to considerable ice loss as deduced from just six meters of ice remaining from this period (blue horizontal line, Fig. 3)~~. It is evident that at the end of the MCA the MPG still preserved ice from the RP and the first half of the DA (Fig. 5D). It is difficult to ~~assure-confirm~~ if Neoglacial basal ice is still present in MPG since no ice sample was dated with Neoglacial age or even older. Still, Neoglacial ice ~~can-could have~~ remained in the glacier base without being exposed by the slope where sampling procedures were carried out.

Over such a diminished MCA glacier, ice started to accumulate again at a rapid rate during the LIA (1300 – 1850 CE). In most cases, the LIA was the period when mountain glaciers recorded their maximum Holocene extent (Solomina et al., 2016), with remarkable advances in ~~the alpine~~ [Alpine](#) glaciers (Ivy-Ochs et al., 2009). From a large

variety of proxies, several warm and cold periods have been identified in the Iberian Peninsula during the LIA (Oliva et al., 2018). In the Marboré Cirque two generations of LIA moraines have been mapped (García-Ruiz et al., 2014), whose emplacement coincided with the coldest LIA phases, i.e. 1620 - 1715 CE, when the Pyrenean glaciers recorded their maximum extent of the last two millennia, and at some time between 1820 - 1840 CE, when a rapid advance of the ice mass moved over the large moraine leaving parallel ridges and furrows, so-called flutes, as signs of erosion (García-Ruiz et al., 2020; Serrano and Martín-Moreno, 2018). These two cold phases are very well identified in the Marboré Cirque and were confirmed by the study of the altitudinal fluctuations of the timberline in the neighboring Escuaín Valley (Camarero et al., 2015). In fact, according to the map of Schrader from 1874 CE and other historical sources, the MPG made direct contact with the large moraine in the second half of the 19th century (García-Ruiz et al., 2014). Despite the fact that the MPG would have covered an area of 5.56 km² at the end of the LIA-LIA (Fig. 5E) (in 1894) (González Trueba et al., 2008), Fig. 5E), there is no record today of ice accumulated during the LIA, except for a few meters at the top of the sequence corresponding to about 1400 CE. This means that more than 600 years of ice accumulation have been lost associated to the with warming after ca. 1850 CE. This situation is not so common in the Alps, where ice from the LIA, and even from the last two centuries, is still commonly preserved in many studied cold glaciers (Eichler et al., 2000; Gabrielli et al., 2016; Gäggeler et al., 1983; Preunkert et al., 2019).

Today the MPG is divided in two small ice bodies that together cover just 0.38 km² (López-Moreno et al., 2016; Fig. 5F). Comparing the MPG extent at the end of the LIA (ca. 1850 CE), as given by the moraine location, and today's extent, more than 5 km² of MPG would have disappeared, thus indicating that the last 150 years have likely been the period with the largest glacier melting over the last 2000 years.

5. Conclusions

This study presents for the first time a continuous chronological model of a remaining small glacier in the Pyrenees, reconstructed from a set of ¹⁴C dates on different organic remains, and supported by measurements of current atmospheric deposition and

comparison with a nearby lake sequence (Marboré Lake). The ice sequence from [the Monte Perdido Glacier \(MPG\)](#) covers the last 2000 years, allowing the identification of cold time periods of ~~growing glaciers~~[glacier growth](#) and warm time periods of ice loss. We demonstrate that the glacier was active during the [Roman Period \(RP\)](#), a well-known warm period in the Iberian Peninsula. During the [Medieval Climate Anomaly \(MCA\)](#), the MPG experienced a ~~spectacular-dramatic~~ retreat marked by the presence of dark debris layers ~~indicative-interpreted in terms~~ of successive years when ablation processes predominated. ~~The~~[The Little Ice Age \(LIA\)](#) was a period of glacier growth, but [it](#) is not recorded today in the ice from MPG, since more than 600 years of ice accumulation have been lost associated to the warming after the end of the LIA, [at](#) ca. 1850 CE. This evidence from the ~~age-depth~~[age](#) model is supported by the lack of anthropogenic indicators usually associated ~~to-with~~ the Industrial Era, [which are](#) abundant today ~~in-in the~~ current atmospheric deposition in a nearby site. Additionally, both [the](#) Hg concentration and [the](#) Pb/Al ratio appear much higher in the Marboré Lake sediments, whereas the MPG record does not reflect their anthropogenic increase.

Comparing the present-day glacier situation with that of previous warm intervals, such as the RP or the MCA, we conclude that the MPG is nowadays greatly reduced in area and volume. Additionally, the recent rate of ice-mass loss is definitely more rapid than that of the four centuries spanned by the MCA, thus suggesting that present day warming in the Pyrenees is faster and more intense than in any previous warm phase of the last 2000 years. Under the current climatic conditions, it is reasonable to expect the disappearance of this glacier, as well as other glaciers in the Pyrenees and in Southern Europe, over the next few decades.

6. Data availability

The input data file for CLAM as well as the output results are stored in the open repository Zenodo (<https://zenodo.org/record/3886911>). The rest of data are given in the paper Tables.

7. Author contributions

570 The paper was conceived by A.M., M.B., C.S. and J.I.L-M. together with F.N., J.O-G., J.L.,
571 P.G-S., C.C., J.L-M., B.O-U, S.H.F and J.G-R. who contributed to design and develop this
572 research project (PaleoICE). F.N., C.P., M.L., E.A. participated during field work to
573 recover the samples; A.M., M.B. and M.L. prepared the samples for ^{14}C dating; J.G.O.
574 carried out the ^{210}Pb and ^{137}Cs analyses; J.P., X.Q. and A.A. provided the geochemical
575 data from Ordesa site and MPG; J.P.C., M.J.S. and R.M. provided the Hg data from
576 Marboré Lake and MPG; and G.G.-R. built the age depth-model. All authors
577 contributed to discuss and interpret the data and to the writing of the original and
578 revised version of this paper.

579 **8. Competing interest**

580 The authors declare that they have no conflict of interest.

581 **9. Acknowledgements**

582 The Spanish Agencia Estatal de Investigación (AEI – Spain) and the European Funds for
583 Regional Development (FEDER – European Union) are gratefully acknowledged for
584 financial support through PaleoICE EXPLORA project (CGL2015-72167-EXP), CGL2015-
585 68993-R, CGL2015-69160-R and CTM2017-84441-R projects (AEI/FEDER, UE) and
586 through the iMechPro RETOS project (RTI2018-100696-B-I00). S.H.F. and J.G.-O.
587 acknowledge support by the Spanish Government through María de Maeztu excellence
588 accreditation 2018-2022 ref MDM-2017-0714 and ref CEX-2019-000940-M,
589 respectively. M.B. is supported by postdoctoral fellowship Juan de la Cierva-Formación
590 program provided by the Spanish Ministry of Science, Innovation and Universities (ref.:
591 FJCI-2017-34235063753). The authors are grateful to Eduardo Bartolomé and José
592 Estebán Lozano for their help manufacturing parts of the coring devices and to the
593 support provided by the Dirección General de Conservación del Medio Natural
594 (Government of Aragón) and by the staff of the Ordesa and Monte Perdido National
595 Park during our field campaigns. This study contributes to the work carried out by the
596 GA research group Procesos Geoambientales y Cambio Global (ref E02-20R) and MERS
597 research group 2017 SGR 1588.

598 **10. References**

Con formato: Inglés (Estados Unidos)

Con formato: Inglés (Estados Unidos)

- 599 Blaauw, M.: Methods and code for 'classical' age-modelling of radiocarbon sequences,
600 Quaternary Geochronology, 5(5), 512–518, <https://doi.org/10.1016/j.quageo.2010.01.002>,
601 2010.
- 602 Blaauw, M., Christen, J. A., Vázquez, J. E. and Goring, S.: clam: Classical Age-Depth Modelling of
603 Cores from Deposits. CRAN 2019, <https://CRAN.R-project.org/package=clam>, 2019.
- 604 Bohleber, P.: Alpine Ice Cores as Climate and Environmental Archives, Oxford Research
605 Encyclopedia of Climate Science, <https://doi.org/10.1093/acrefore/9780190228620.013.743>,
606 2019.
- 607 Bohleber, P., Schwikowski, M., Stocker-Waldhuber, M., Fang, L. and Fischer, A.: New glacier
608 evidence for ice-free summits during the life of the Tyrolean Iceman, Sci Rep, 10(1), 20513,
609 <https://doi.org/10.1038/s41598-020-77518-9>, 2020.
- 610 Büntgen, U., Krusic, P. J., Verstege, A., Sangüesa-Barreda, G., Wagner, S., Camarero, J. J.,
611 Ljungqvist, F. C., Zorita, E., Oppenheimer, C., Konter, O., Tegel, W., Gärtner, H., Cherubini, P.,
612 Reinig, F. and Esper, J.: New Tree-Ring Evidence from the Pyrenees Reveals Western
613 Mediterranean Climate Variability since Medieval Times, J. Climate, 30(14), 5295–5318,
614 <https://doi.org/10.1175/JCLI-D-16-0526.1>, 2017.
- 615 Callén, J. J. N.: El proceso sidero-metarlúrgico altoaragonés: los valles de Bielsa y Gistain en la
616 Edad Moderna (1565-1800), Lull: Revista de la Sociedad Española de Historia de las Ciencias y
617 de las Técnicas, 19(37), 471–508, 1996.
- 618 Camarero, J. J., García-Ruiz, J. M., Sangüesa-Barreda, G., Galván, J. D., Alla, A. Q., Sanjuán, Y.,
619 Beguería, S. and Gutiérrez, E.: Recent and Intense Dynamics in a Formerly Static Pyrenean
620 Treeline, Arctic, Antarctic, and Alpine Research, 47(4), 773–783,
621 <https://doi.org/10.1657/AAAR0015-001>, 2015.
- 622 Cisneros, M., Cacho, I., Frigola, J., Canals, M., Masqué, P., Martrat, B., Casado, M., Grimalt, J.
623 O., Pena, L. D., Margaritelli, G. and Lirer, F.: Sea surface temperature variability in the central-
624 western Mediterranean Sea during the last 2700 years: a multi-proxy and multi-record
625 approach, Clim. Past, 12(4), 849–869, <https://doi.org/10.5194/cp-12-849-2016>, 2016.
- 626 Cooke, C. A., Martínez-Cortizas, A., Bindler, R. and Sexauer Gustin, M.: Environmental archives
627 of atmospheric Hg deposition – A review, Science of The Total Environment, 709, 134800,
628 <https://doi.org/10.1016/j.scitotenv.2019.134800>, 2020.
- 629 Corella, J. P., Valero-Garcés, B. L., Vicente-Serrano, S. M., Brauer, A. and Benito, G.: Three
630 millennia of heavy rainfalls in Western Mediterranean: frequency, seasonality and atmospheric
631 drivers, Scientific Reports, 6(1), <https://doi.org/10.1038/srep38206>, 2016.
- 632 Corella, J. P., Saiz-Lopez, A., Sierra, M. J., Mata, M. P., Millán, R., Morellón, M., Cuevas, C. A.,
633 Moreno, A. and Valero-Garcés, B. L.: Trace metal enrichment during the Industrial Period
634 recorded across an altitudinal transect in the Southern Central Pyrenees, Science of The Total
635 Environment, 645, 761–772, <https://doi.org/10.1016/j.scitotenv.2018.07.160>, 2018.
- 636 Corella, J. P., Sierra, M. J., Garralón, A., Millán, R., Rodríguez-Alonso, J., Mata, M. P., de Vera, A.
637 V., Moreno, A., González-Sampériz, P., Duval, B., Amouroux, D., Vivez, P., Cuevas, C. A., Adame,
638 J. A., Wilhelm, B., Saiz-Lopez, A. and Valero-Garcés, B. L.: Recent and historical pollution legacy
639 in high altitude Lake Marboré (Central Pyrenees): A record of mining and smelting since pre-

640 Roman times in the Iberian Peninsula, *Science of The Total Environment*, 751, 141557,
641 <https://doi.org/10.1016/j.scitotenv.2020.141557>, 2021.

642 Davis, P. T., Menounos, B. and Osborn, G.: Holocene and latest Pleistocene alpine glacier
643 fluctuations: a global perspective, *Quaternary Science Reviews*, 28(21–22), 2021–2033,
644 <https://doi.org/10.1016/j.quascirev.2009.05.020>, 2009.

645 Di Stefano, E., Clemenza, M., Baccolo, G., Delmonte, B. and Maggi, V.: 137Cs contamination in
646 the Adamello glacier: Improving the analytical method, *Journal of Environmental Radioactivity*,
647 208–209, 106039, <https://doi.org/10.1016/j.jenvrad.2019.106039>, 2019.

648 Eichler, A., Schwikowski, M., Gäggeler, H. W., Furrer, V., Synal, H.-A., Beer, J., Saurer, M. and
649 Funk, M.: Glaciochemical dating of an ice core from upper Grenzgletscher (4200 m a.s.l.),
650 *Journal of Glaciology*, 46(154), 507–515, <https://doi.org/10.3189/172756500781833098>, 2000.

651 Ewing, M. E., Reese, C. A. and Nolan, M. A.: The potential effects of percolating snowmelt on
652 palynological records from firn and glacier ice, *Journal of Glaciology*, 60(222), 661–669,
653 <https://doi.org/10.3189/2014JoG13J158>, 2014.

654 Festi, D., Carturan, L., Kofler, W., dalla Fontana, G., de Blasi, F., Cazorzi, F., Bucher, E., Mair, V.,
655 Gabrielli, P. and Oegg, K.: Linking pollen deposition and snow accumulation on the Alto
656 dell'Ortles glacier (South Tyrol, Italy) for sub-seasonal dating of a firn temperate core, *The*
657 *Cryosphere*, 11(2), 937–948, <https://doi.org/10.5194/tc-11-937-2017>, 2017.

658 Festi, D., Schwikowski, M., Maggi, V., Oegg, K. and Jenk, T. M.: Significant mass loss in the
659 accumulation area of the Adamello glacier indicated by the chronology of a 46&thinspm ice
660 core, *The Cryosphere Discussions*, 1–13, <https://doi.org/10.5194/tc-2020-334>, 2020.

661 Fletcher, W. J., Zielhofer, C., Mischke, S., Bryant, C., Xu, X. and Fink, D.: AMS radiocarbon
662 dating of pollen concentrates in a karstic lake system, *Quaternary Geochronology*, 39, 112–
663 123, <https://doi.org/10.1016/j.quageo.2017.02.006>, 2017.

664 Gabrieli, J., Carturan, L., Gabrielli, P., Kehrwald, N., Turetta, C., Cozzi, G., Spolaor, A., Dinale, R.,
665 Staffler, H., Seppi, R., dalla Fontana, G., Thompson, L. and Barbante, C.: Impact of Po Valley
666 emissions on the highest glacier of the Eastern European Alps, *Atmospheric Chemistry and*
667 *Physics*, 11(15), 8087–8102, <https://doi.org/10.5194/acp-11-8087-2011>, 2011.

668 Gabrielli, P., Barbante, C., Bertagna, G., Bertó, M., Binder, D., Carton, A., Carturan, L., Cazorzi,
669 F., Cozzi, G., Dalla Fontana, G., Davis, M., De Blasi, F., Dinale, R., Dragà, G., Dreossi, G., Festi, D.,
670 Frezzotti, M., Gabrieli, J., Galos, S. P., Ginot, P., Heidenwolf, P., Jenk, T. M., Kehrwald, N.,
671 Kenny, D., Magand, O., Mair, V., Mikhalenko, V., Lin, P. N., Oegg, K., Piffer, G., Rinaldi, M.,
672 Schotterer, U., Schwikowski, M., Seppi, R., Spolaor, A., Stenni, B., Tonidandel, D., Uglietti, C.,
673 Zagorodnov, V., Zanoner, T. and Zennaro, P.: Age of the Mt. Ortles ice cores, the Tyrolean
674 Iceman and glaciation of the highest summit of South Tyrol since the Northern Hemisphere
675 Climatic Optimum, *The Cryosphere*, 10(6), 2779–2797, [https://doi.org/10.5194/tc-10-2779-](https://doi.org/10.5194/tc-10-2779-2016)
676 2016, 2016.

677 Gäggeler, H., Gunten, H. R. von, Rössler, E., Oeschger, H. and Schotterer, U.: 210Pb-Dating of
678 Cold Alpine Firn/Ice Cores From Colle Gnifetti, Switzerland, *Journal of Glaciology*, 29(101),
679 165–177, <https://doi.org/10.1017/S0022143000005220>, 1983.

680 Gaggeler, H. W., Tobler, L., Schwikowski, M. and Jenk, T. M.: Application of the radionuclide
681 ^{210}Pb in glaciology – an overview, *Journal of Glaciology*, 66(257), 447–456,
682 <https://doi.org/10.1017/jog.2020.19>, 2020.

683 García-Ruiz, J. M., Palacios, D., Andrés, N. de, Valero-Garcés, B. L., López-Moreno, J. I. and
684 Sanjuán, Y.: Holocene and ‘Little Ice Age’ glacial activity in the Marboré Cirque, Monte Perdido
685 Massif, Central Spanish Pyrenees, *The Holocene*, 0959683614544053,
686 <https://doi.org/10.1177/0959683614544053>, 2014.

687 García-Ruiz, J. M., Palacios, D., Andrés, N. and López-Moreno, J. I.: Neoglaciation in the Spanish
688 Pyrenees: a multiproxy challenge, *Med. Geosc. Rev.*, 2(1), 21–36,
689 <https://doi.org/10.1007/s42990-020-00022-9>, 2020.

690 Garzonio, R., Di Mauro, B., Strigaro, D., Rossini, M., Colombo, R., De Amicis, M. and Maggi, V.:
691 Mapping the suitability for ice-core drilling of glaciers in the European Alps and the Asian High
692 Mountains, *J. Glaciol.*, 64(243), 12–26, <https://doi.org/10.1017/jog.2017.75>, 2018.

693 González Trueba, J. J., Moreno, R. M., Martínez de Pisón, E. and Serrano, E.: ‘Little Ice Age’
694 glaciation and current glaciers in the Iberian Peninsula, *The Holocene*, 18(4), 551–568,
695 <https://doi.org/10.1177/0959683608089209>, 2008.

696 Haeberli, W., Gaggeler, H., Baltensperger, U., Jost, D. and Schotterer, U.: The Signal from the
697 Chernobyl Accident in High-Altitude Firn Areas of the Swiss Alps, *Annals of Glaciology*, 10, 48–
698 51, <https://doi.org/10.3189/S0260305500004158>, 1988.

699 Haeberli, W., Frauenfelder, R., Kääb, A. and Wagner, S.: Characteristics and potential climatic
700 significance of “miniature ice caps” (crest- and cornice-type low-altitude ice archives), *Journal*
701 *of Glaciology*, 50(168), 129–136, <https://doi.org/10.3189/172756504781830330>, 2004.

702 Herren, P.-A., Eichler, A., Machguth, H., Papina, T., Tobler, L., Zapf, A. and Schwikowski, M.: The
703 onset of Neoglaciation 6000 years ago in western Mongolia revealed by an ice core from the
704 Tsambagarav mountain range, *Quaternary Science Reviews*, 69, 59–68,
705 <https://doi.org/10.1016/j.quascirev.2013.02.025>, 2013.

706 Holzhauser, H., Magny, M. and Zumbühl, H. J.: Glacier and lake-level variations in west-central
707 Europe over the last 3500 years, *The Holocene*, 15(6), 789–801, 2005.

708 Hughes, P. D.: Little Ice Age glaciers and climate in the Mediterranean mountains: a new
709 analysis, *CIG*, 44(1), 15, <https://doi.org/10.18172/cig.3362>, 2018.

710 Ivy-Ochs, S., Kerschner, H., Maisch, M., Christl, M., Kubik, P. W. and Schlüchter, C.: Latest
711 Pleistocene and Holocene glacier variations in the European Alps, *Quaternary Science Reviews*,
712 28(21–22), 2137–2149, <https://doi.org/10.1016/j.quascirev.2009.03.009>, 2009.

713 Jenk, T. M., Szidat, S., Boliu, D., Sigl, M., Gaggeler, H. W., Wacker, L., Ruff, M., Barbante, C.,
714 Boutron, C. F. and Schwikowski, M.: A novel radiocarbon dating technique applied to an ice
715 core from the Alps indicating late Pleistocene ages, *Journal of Geophysical Research:*
716 *Atmospheres*, 114(D14), <https://doi.org/10.1029/2009JD011860>, 2009.

717 Kilian, M. R., van der Plicht, J., van Geel, B. and Goslar, T.: Problematic ^{14}C -AMS dates of pollen
718 concentrates from Lake Gosiaz (Poland), *Quaternary International*, 88(1), 21–26,
719 [https://doi.org/10.1016/S1040-6182\(01\)00070-2](https://doi.org/10.1016/S1040-6182(01)00070-2), 2002.

720 Leunda, M., González-Sampériz, P., Gil-Romera, G., Aranbarri, J., Moreno, A., Oliva-Urcia, B.,
721 Sevilla-Callejo, M. and Valero-Garcés, B.: The Late-Glacial and Holocene Marboré Lake
722 sequence (2612m a.s.l., Central Pyrenees, Spain): Testing high altitude sites sensitivity to
723 millennial scale vegetation and climate variability, *Global and Planetary Change*, 157, 214–231,
724 <https://doi.org/10.1016/j.gloplacha.2017.08.008>, 2017.

725 López-Moreno, J. I., Revuelto, J., Rico, I., Chueca-Cía, J., Julián, A., Serreta, A., Serrano, E.,
726 Vicente-Serrano, S. M., Azorin-Molina, C., Alonso-González, E. and García-Ruiz, J. M.: Thinning
727 of the Monte Perdido Glacier in the Spanish Pyrenees since 1981, *The Cryosphere*, 10(2), 681–
728 694, <https://doi.org/10.5194/tc-10-681-2016>, 2016.

729 López-Moreno, J. I., Alonso-González, E., Monserrat, O., Del Río, L. M., Otero, J., Lapazaran, J.,
730 Luzi, G., Dematteis, N., Serreta, A., Rico, I., Serrano-Cañadas, E., Bartolomé, M., Moreno, A.,
731 Buisan, S. and Revuelto, J.: Ground-based remote-sensing techniques for diagnosis of the
732 current state and recent evolution of the Monte Perdido Glacier, Spanish Pyrenees, *J. Glaciol.*,
733 65(249), 85–100, <https://doi.org/10.1017/jog.2018.96>, 2019.

734 Mann, M. E., Zhang, Z., Rutherford, S., Bradley, R. S., Hughes, M. K., Shindell, D., Ammann, C.,
735 Faluvegi, G. and Ni, F.: Global Signatures and Dynamical Origins of the Little Ice Age and
736 Medieval Climate Anomaly, *Science*, 326(5957), 1256–1260, 2009.

737 Margaritelli, G., Cacho, I., Català, A., Barra, M., Bellucci, L. G., Lubritto, C., Rettori, R. and Lirer,
738 F.: Persistent warm Mediterranean surface waters during the Roman period, *Scientific Reports*,
739 10(1), 10431, <https://doi.org/10.1038/s41598-020-67281-2>, 2020.

740 Martín-Puertas, C., Jiménez-Espejo, F., Martínez-Ruiz, F., Nieto-Moreno, V., Rodrigo, M., Mata,
741 M. P. and Valero-Garcés, B. L.: Late Holocene climate variability in the southwestern
742 Mediterranean region: an integrated marine and terrestrial geochemical approach, *Clim. Past*,
743 6(6), 807–816, <https://doi.org/10.5194/cp-6-807-2010>, 2010.

744 Marzeion, B., Cogley, J. G., Richter, K. and Parkes, D.: Attribution of global glacier mass loss to
745 anthropogenic and natural causes, *Science*, 345(6199), 919–921,
746 <https://doi.org/10.1126/science.1254702>, 2014.

747 Moore, P. D., Webb, J. A. and Collinson, M. E.: *Pollen Analysis, Second.*, Blackwell Scientific
748 Publications., 1991.

749 More, A. F., Spaulding, N. E., Bohleber, P., Handley, M. J., Hoffmann, H., Korotkikh, E. V.,
750 Kurbatov, A. V., Loveluck, C. P., Sneed, S. B., McCormick, M. and Mayewski, P. A.: Next-
751 generation ice core technology reveals true minimum natural levels of lead (Pb) in the
752 atmosphere: Insights from the Black Death, *GeoHealth*, 1(4), 211–219,
753 <https://doi.org/10.1002/2017GH000064>, 2017.

754 Morellón, M., Valero-Garcés, B., Vegas-Vilarrúbia, T., González-Sampériz, P., Romero, Ó.,
755 Delgado-Huertas, A., Mata, P., Moreno, A., Rico, M. and Corella, J. P.: Lateglacial and Holocene
756 palaeohydrology in the western Mediterranean region: The Lake Estanya record (NE Spain),
757 *Quaternary Science Reviews*, 28(25–26), 2582–2599, 2009.

758 Oerlemans, J.: *Glaciers and Climate Change*, CRC Press., 2001.

759 Oliva, M., Ruiz-Fernández, J., Barriendos, M., Benito, G., Cuadrat, J. M., Domínguez-Castro, F.,
760 García-Ruiz, J. M., Giralt, S., Gómez-Ortiz, A., Hernández, A., López-Costas, O., López-Moreno,
761 J. I., López-Sáez, J. A., Martínez-Cortizas, A., Moreno, A., Prohom, M., Saz, M. A., Serrano, E.,

762 Tejedor, E., Trigo, R., Valero-Garcés, B. and Vicente-Serrano, S. M.: The Little Ice Age in Iberian
763 mountains, *Earth-Science Reviews*, 177, 175–208,
764 <https://doi.org/10.1016/j.earscirev.2017.11.010>, 2018.

765 Oliva-Urcia, B., Moreno, A., Leunda, M., Valero-Garcés, B., González-Sampériz, P., Gil-Romera,
766 G., Mata, M. P. and Group, H.: Last deglaciation and Holocene environmental change at high
767 altitude in the Pyrenees: the geochemical and paleomagnetic record from Marboré Lake (N
768 Spain), *J Paleolimnol*, 59(3), 349–371, <https://doi.org/10.1007/s10933-017-0013-9>, 2018.

769 Palacios, D., García-Ruiz, J. M., Andrés, N., Schimmelpfennig, I., Campos, N., Léanni, L.,
770 Aumaître, G., Bourlès, D. L. and Keddadouche, K.: Deglaciation in the central Pyrenees during
771 the Pleistocene–Holocene transition: Timing and geomorphological significance, *Quaternary*
772 *Science Reviews*, 162, 111–127, <https://doi.org/10.1016/j.quascirev.2017.03.007>, 2017.

773 Pey, J., Pérez, N., Cortés, J., Alastuey, A. and Querol, X.: Chemical fingerprint and impact of
774 shipping emissions over a western Mediterranean metropolis: Primary and aged contributions,
775 *Science of The Total Environment*, 463–464, 497–507,
776 <https://doi.org/10.1016/j.scitotenv.2013.06.061>, 2013.

777 Pey, J., Larrasoaña, J. C., Pérez, N., Cerro, J. C., Castillo, S., Tobar, M. L., de Vergara, A.,
778 Vázquez, I., Reyes, J., Mata, M. P., Mochales, T., Orellana, J. M. and Causapé, J.:
779 Phenomenology and geographical gradients of atmospheric deposition in southwestern
780 Europe: Results from a multi-site monitoring network, *Science of The Total Environment*, 744,
781 140745, <https://doi.org/10.1016/j.scitotenv.2020.140745>, 2020.

782 Pohjola, V. A., Moore, J. C., Isaksson, E., Jauhiainen, T., Wal, R. S. W. van de, Martma, T.,
783 Meijer, H. a. J. and Vaikmäe, R.: Effect of periodic melting on geochemical and isotopic signals
784 in an ice core from Lomonosovfonna, Svalbard, *Journal of Geophysical Research: Atmospheres*,
785 107(D4), ACL 1-1-ACL 1-14, <https://doi.org/10.1029/2000JD000149>, 2002.

786 Preunkert, S., McConnell, J. R., Hoffmann, H., Legrand, M., Wilson, A. I., Eckhardt, S., Stohl, A.,
787 Chellman, N. J., Arienzo, M. M. and Friedrich, R.: Lead and Antimony in Basal Ice From Col du
788 Dome (French Alps) Dated With Radiocarbon: A Record of Pollution During Antiquity,
789 *Geophysical Research Letters*, 46(9), 4953–4961, <https://doi.org/10.1029/2019GL082641>,
790 2019.

791 Querol, X., Viana, M., Alastuey, A., Amato, F., Moreno, T., Castillo, S., Pey, J., de la Rosa, J.,
792 Sánchez de la Campa, A., Artíñano, B., Salvador, P., García Dos Santos, S., Fernández-Patier, R.,
793 Moreno-Grau, S., Negral, L., Minguillón, M. C., Monfort, E., Gil, J. I., Inza, A., Ortega, L. A.,
794 Santamaría, J. M. and Zabalza, J.: Source origin of trace elements in PM from regional
795 background, urban and industrial sites of Spain, *Atmospheric Environment*, 41(34), 7219–7231,
796 <https://doi.org/10.1016/j.atmosenv.2007.05.022>, 2007.

797 Reimer, P. J., Bard, E., Bayliss, A., Beck, J. W., Blackwell, P. G., Ramsey, C. B., Buck, C. E., Cheng,
798 H., Edwards, R. L., Friedrich, M., and others: IntCal13 and Marine13 radiocarbon age
799 calibration curves 0–50,000 years cal BP, *Radiocarbon*, 55(4), 1869–1887, 2013.

800 Rico, I., Izagirre, E., Serrano, E. and López-Moreno, J. I.: Superficie glaciar actual en los Pirineos:
801 Una actualización para 2016, *Pirineos*, 172(0), 029,
802 <https://doi.org/10.3989/Pirineos.2017.172004>, 2017.

Con formato: Inglés (Estados Unidos)

- 803 Salazar, A., Mata, M. P., Rico, M., Valero-Garcés, Oliva-Urcia, B. and Rubio, F. M.: El paleolago
804 de La Larri (Valle de Pineta, Pirineos), Cuadernos de Investigación Geográfica, 39(1), 97–116,
805 2013.
- 806 Sanchez-Cabeza, J. A., Masqué, P. and Ani-Ragolta, I.: 210Pb and 210Po analysis in sediments
807 and soils by microwave acid digestion, J Radioanal Nucl Chem, 227(1), 19–22,
808 <https://doi.org/10.1007/BF02386425>, 1998.
- 809 Serrano, E. and Martín-Moreno, R.: Surge glaciers during the Little Ice Age in the Pyrenees,
810 Cuadernos de Investigación Geográfica, 44(1), 213–244, <https://doi.org/10.18172/cig.3399>,
811 2018.
- 812 Serrano, E., López-Moreno, J. I., Gómez-Lende, M., Pisabarro, A., Martín-Moreno, R., Rico, I.
813 and Alonso-González, E.: Frozen ground and periglacial processes relationship in temperate
814 high mountains: a case study at Monte Perdido-Tucarroya area (The Pyrenees, Spain), J. Mt.
815 Sci., 17(5), 1013–1031, <https://doi.org/10.1007/s11629-019-5614-5>, 2020.
- 816 Solomina, O. N., Bradley, R. S., Hodgson, D. A., Ivy-Ochs, S., Jomelli, V., Mackintosh, A. N.,
817 Nesje, A., Owen, L. A., Wanner, H., Wiles, G. C. and Young, N. E.: Holocene glacier fluctuations,
818 Quaternary Science Reviews, 111, 9–34, <https://doi.org/10.1016/j.quascirev.2014.11.018>,
819 2015.
- 820 Solomina, O. N., Bradley, R. S., Jomelli, V., Geirsdottir, A., Kaufman, D. S., Koch, J., McKay, N. P.,
821 Masiokas, M., Miller, G., Nesje, A., Nicolussi, K., Owen, L. A., Putnam, A. E., Wanner, H., Wiles,
822 G. and Yang, B.: Glacier fluctuations during the past 2000 years, Quaternary Science Reviews,
823 149, 61–90, <https://doi.org/10.1016/j.quascirev.2016.04.008>, 2016.
- 824 Taylor, S. R. and McLennan, S. M.: The geochemical evolution of the continental crust, Reviews
825 of Geophysics, 33, 241–265, 1995.
- 826 Uglietti, C., Zapf, A., Jenk, T. M., Sigl, M., Szidat, S., Salazar, G. and Schwikowski, M.:
827 Radiocarbon dating of glacier ice: overview, optimisation, validation and potential, The
828 Cryosphere, 10(6), 3091–3105, <https://doi.org/10.5194/tc-10-3091-2016>, 2016.
- 829 Wanner, H., Solomina, O., Grosjean, M., Ritz, S. P. and Jetel, M.: Structure and origin of
830 Holocene cold events, Quaternary Science Reviews, 30(21–22), 3109–3123,
831 <https://doi.org/10.1016/j.quascirev.2011.07.010>, 2011.
- 832 Zemp, M., Frey, H., Gärtner-Roer, I., Nussbaumer, S. U., Hoelzle, M., Paul, F., Haeberli, W.,
833 Denzinger, F., Ahlstrøm, A. P., Anderson, B., Bajracharya, S., Baroni, C., Braun, L. N., Cáceres, B.
834 E., Casassa, G., Cobos, G., Dávila, L. R., Granados, H. D., Demuth, M. N., Espizua, L., Fischer, A.,
835 Fujita, K., Gadek, B., Ghazanfar, A., Hagen, J. O., Holmlund, P., Karimi, N., Li, Z., Pelto, M., Pitte,
836 P., Popovnin, V. V., Portocarrero, C. A., Prinz, R., Sangewar, C. V., Severskiy, I., Sigurdsson, O.,
837 Soruco, A., Usabaliyev, R. and Vincent, C.: Historically unprecedented global glacier decline in
838 the early 21st century, Journal of Glaciology, 61(228), 745–762,
839 <https://doi.org/10.3189/2015JoG15J017>, 2015.
- 840 Zemp, M., Huss, M., Thibert, E., Eckert, N., McNabb, R., Huber, J., Barandun, M., Machguth, H.,
841 Nussbaumer, S. U., Gärtner-Roer, I., Thomson, L., Paul, F., Maussion, F., Kutuzov, S. and Cogley,
842 J. G.: Global glacier mass changes and their contributions to sea-level rise from 1961 to 2016,
843 Nature, 568(7752), 382–386, <https://doi.org/10.1038/s41586-019-1071-0>, 2019.

844

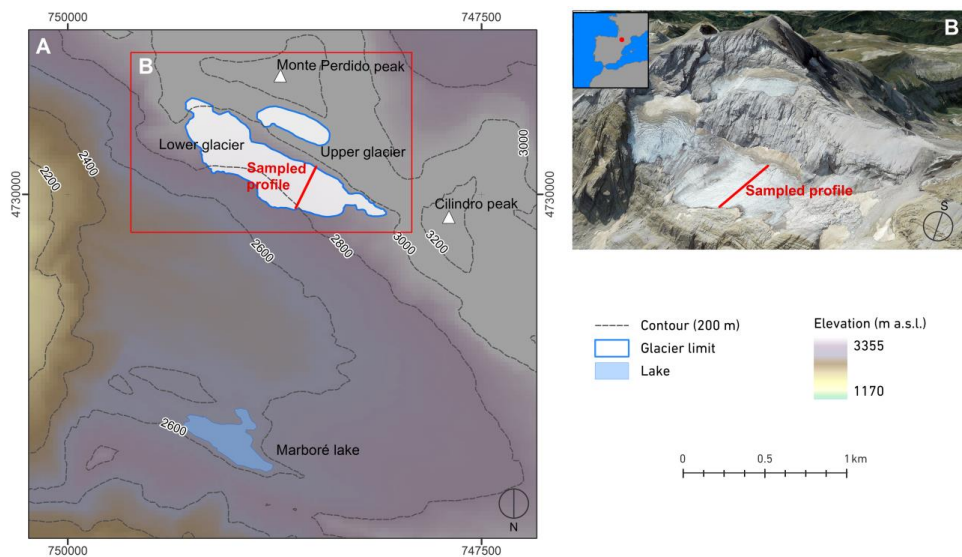
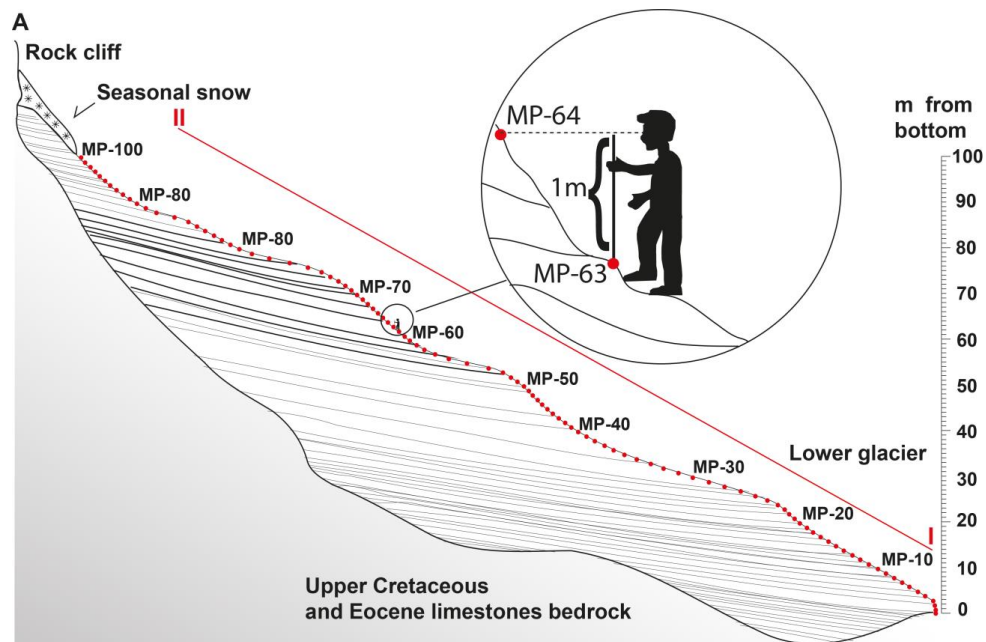
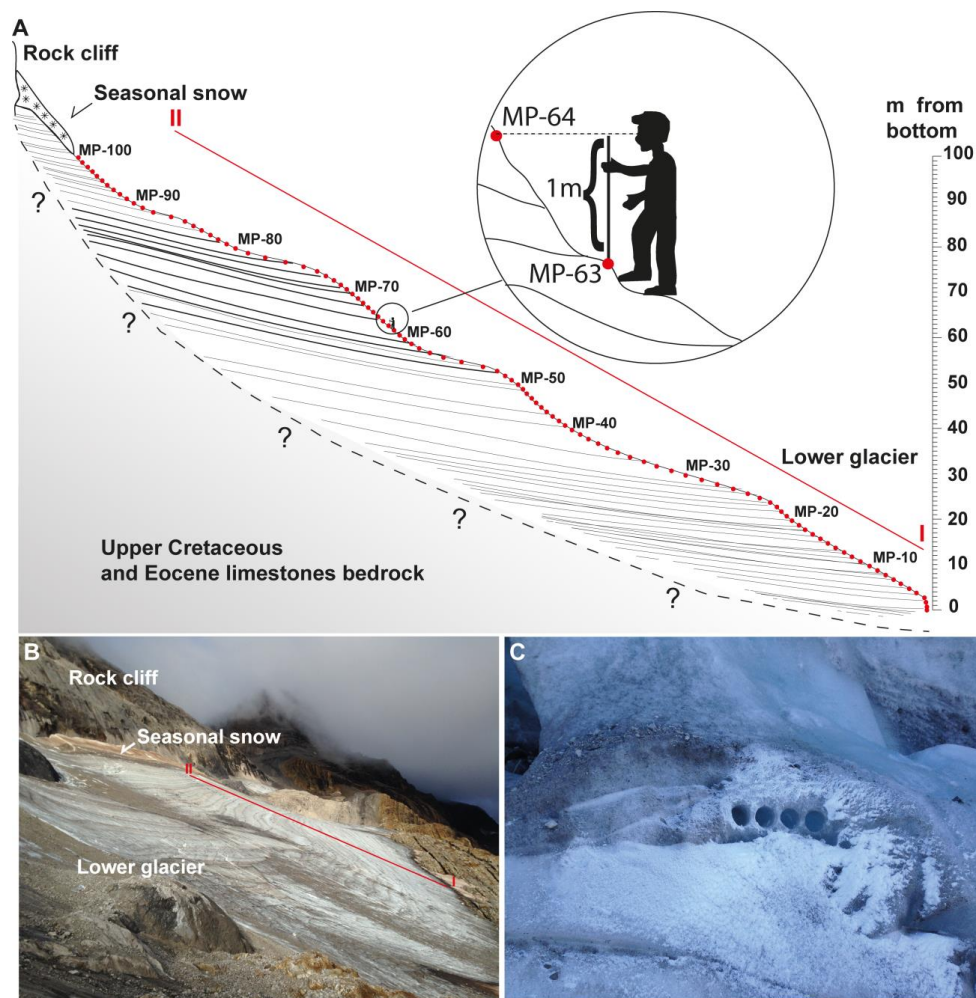


Figure 1. (left A) Location of Monte Perdido Glacier (MPG) within a digital elevation map of Marboré Cirque; (right B) Picture (©Google Earth) of MPG where the location of the sampled profile is indicated (see Fig. 2).



853



Con formato: Interlineado: 1,5 líneas

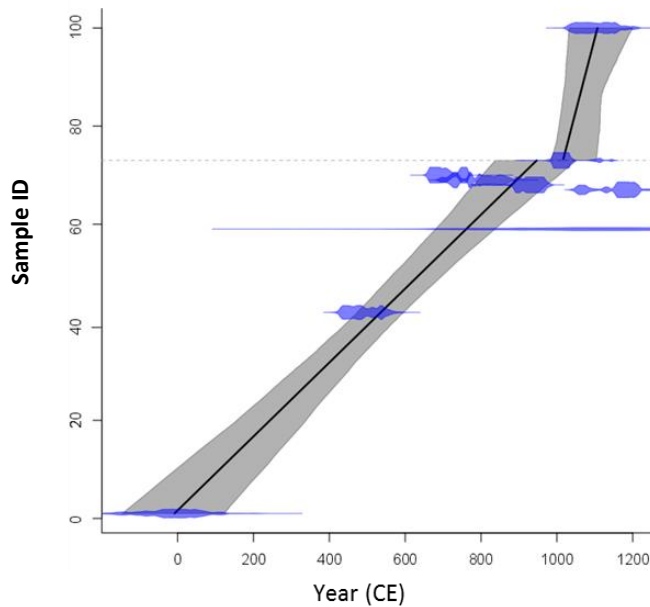
Figure 2. (A) Simplified scheme with the position of the 100 samples collected along the slope (red line I-II marks the profile indicated in B; identification of the samples is MP-0 to MP-100). According to the ice bedding (tilt is approximate) the oldest material should be found at the bottom of the lower glacier. Note the inset with a detailed view of the sampling procedure measuring a height difference of 1 m to obtain every sample. The number of glacier layers is drawn according to the layers observed in the image depicted in (B). Note the inset with a detailed view of the sampling procedure measuring a height difference of 1 m to obtain every sample. (B) Image of the Monte Perdido glacier surface where the sampling was carried out (red line I-II represents the sampled profile shown in Figure 1). Note the presence of dark debris-rich layers

865 alternating with cleaner ice. (C). Detailed view indicating that every sample consisted
866 in 3-4 small horizontally-drilled cylinders (see text for more details).

867

Con formato: Interlineado: 1,5 líneas

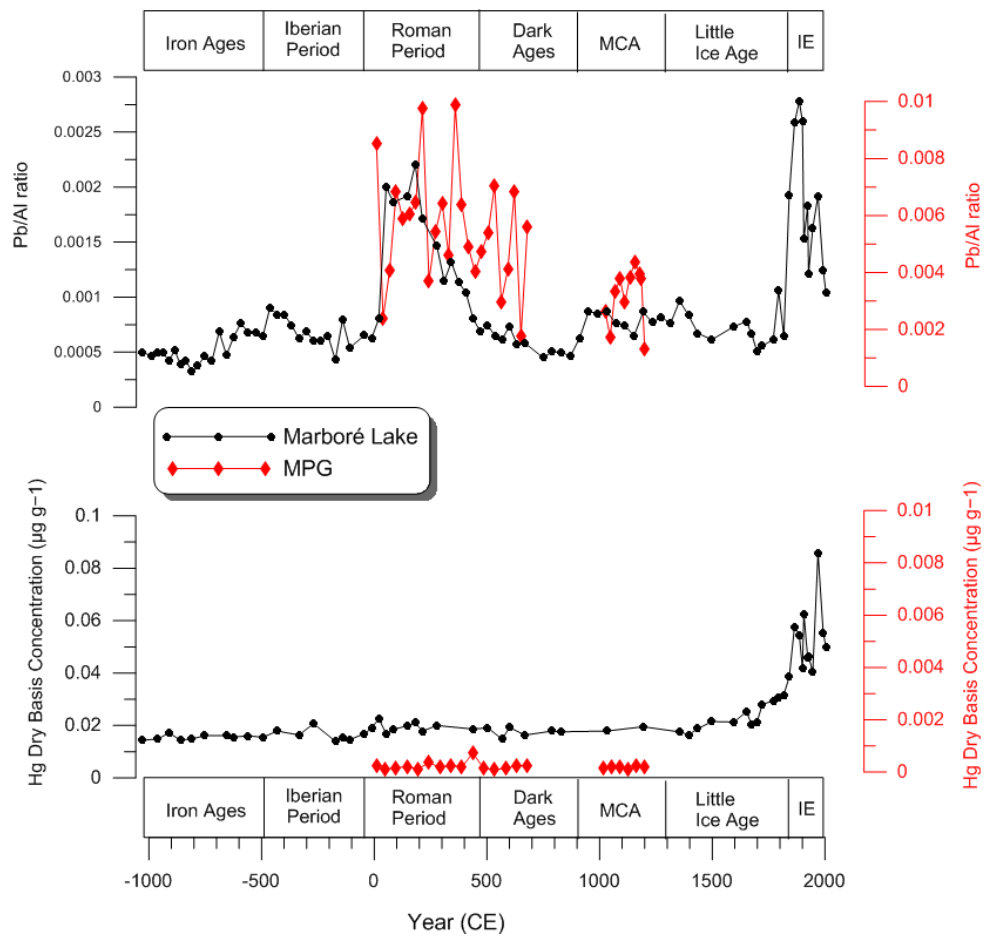
868



869

870 **Figure 3.** Age model for the Monte Perdido ice sequence based on linear interpolation
871 of ^{14}C data (Table 3), obtained using the Clam software (Blaauw, 2010; Blaauw et al.,
872 2019). Y axis indicates the number of samples from MP-0 to MP-100 (see Fig. 2). The
873 dates appear as the calendar-age probability distributions in blue, while the black line
874 is the resulting depth-age model and the gray envelope shows the 95 % confidence
875 interval. Note the hiatus located at 73 m indicated by a dashed line. The error of
876 sample MP59m is so high that appears as a horizontal line.

877



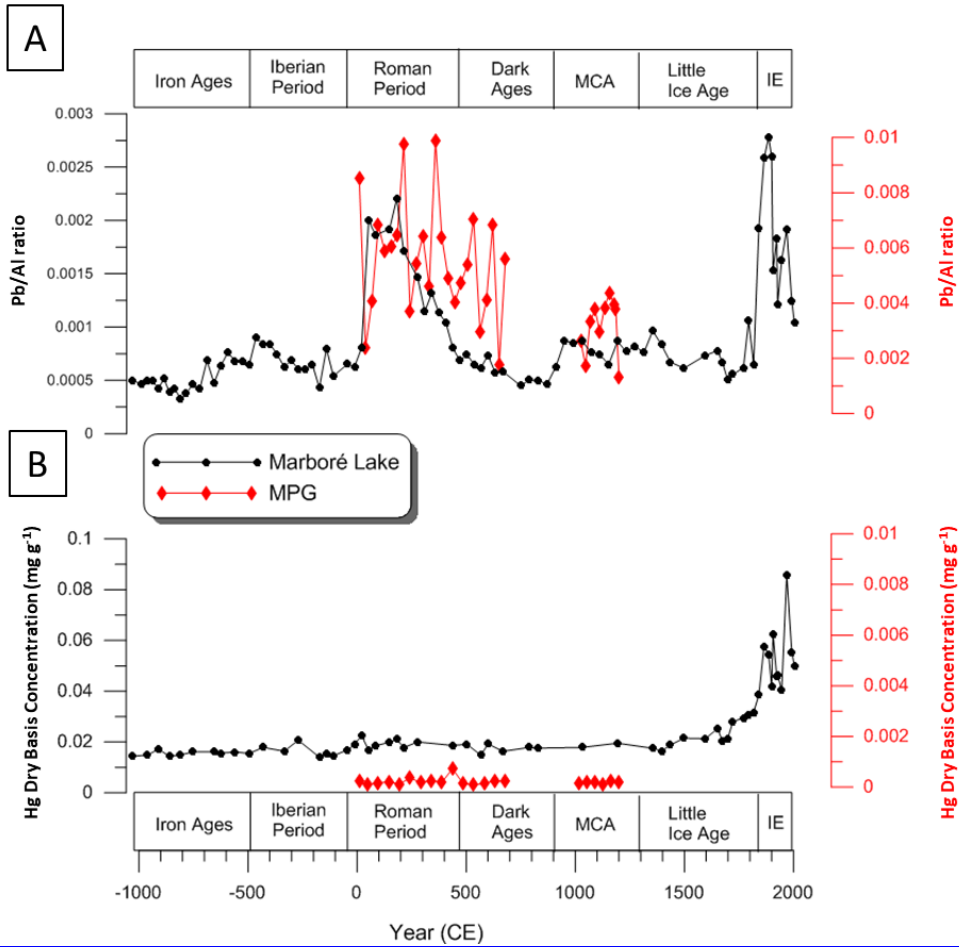
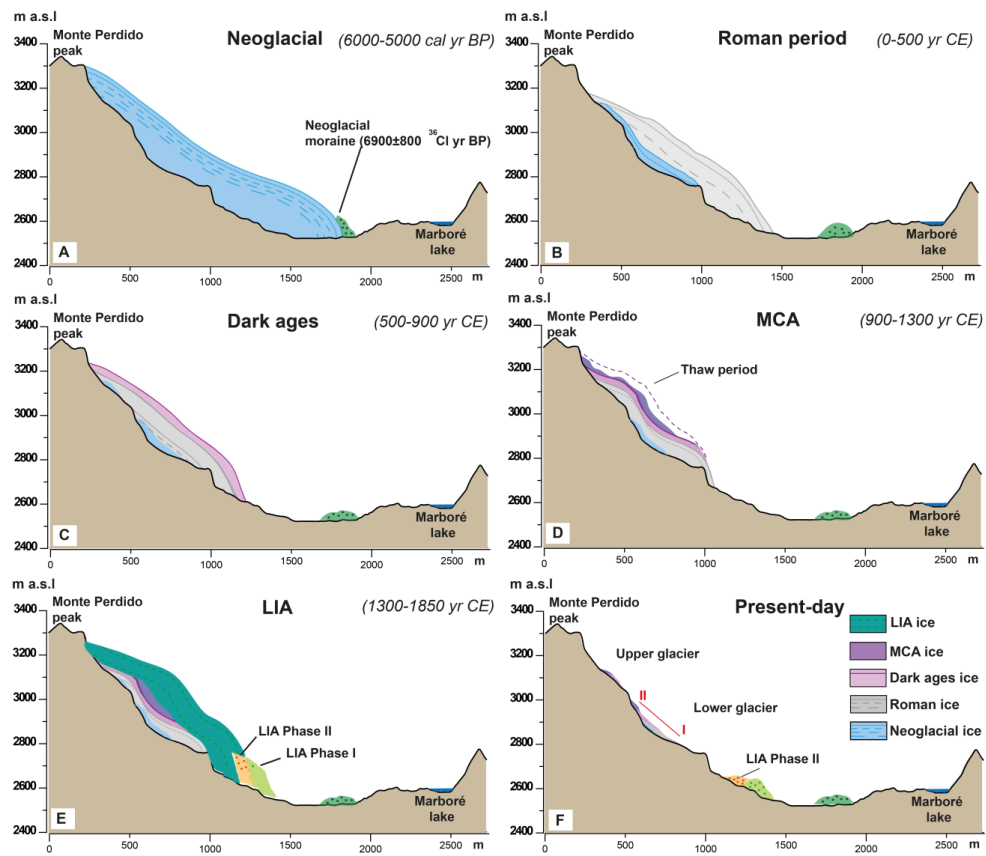


Figure 4. Comparison of Pb/Al ratio and Hg concentration of dry weight sediment in MPG samples with data obtained from Marboré Lake sediments (Corella et al., 2021). Note the differences in the vertical axis. [Sample IDs from MPG are indicated in Table 5.](#)

884



885

886

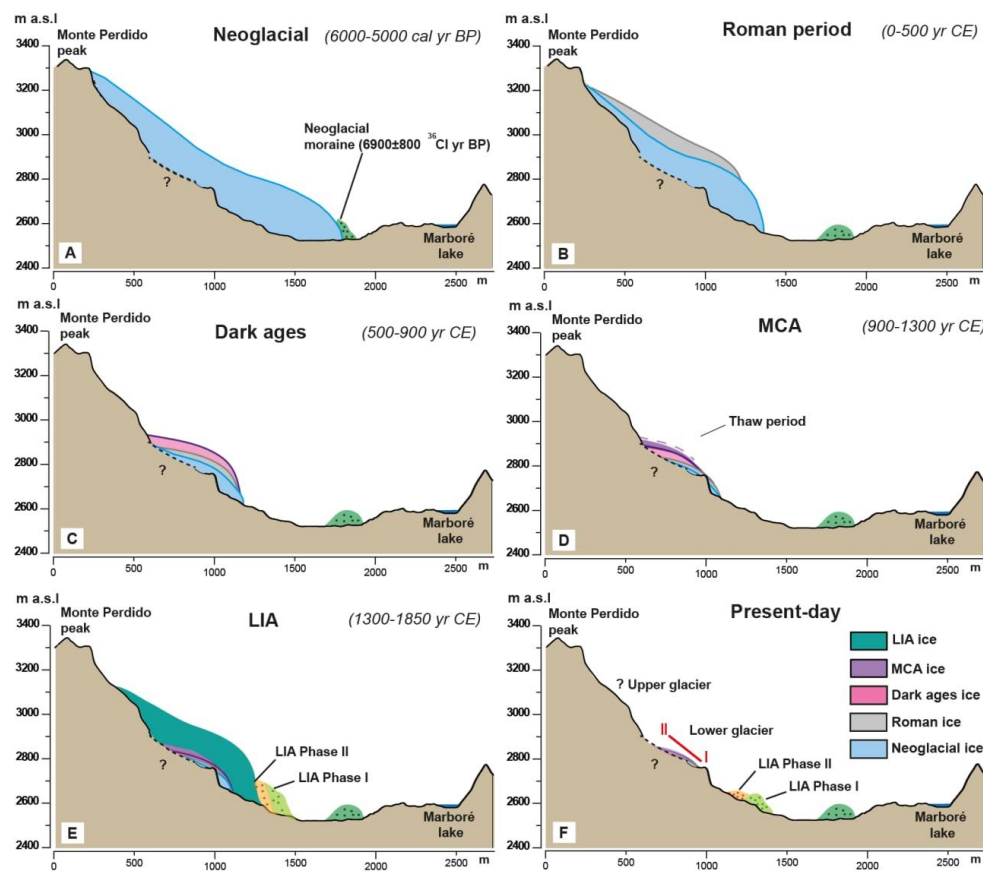


Figure 5. Schematic Ggeomorphic transects (south to north) taken from the Marboré
Cirque, showing the tentative reconstruction of MPG during the six main stages
discussed in the text. A) Neoglacial Period (ca. 5000 – 6000 cal yr BP) where the
Neoglacial moraine is indicated (García-Ruiz et al., 2014); (García-Ruiz et al., 2014). This
figure represents the state of maximum glacier advance during the Neoglacial period.
(B) Roman Period (0-500 CE) when the glacier is shown considerably retreated; (C)
Dark Ages (500-900 CE); (D) Medieval Climate Anomaly (900-1300 CE), a period when
the glacier retreated and ablation caused a concentration of debris and organic
remains form dark layers in the glacier ice (discontinuous line aims to highlight the
importance of melting processes); (E) Little Ice Age (1300-1850 CE), with the MPG
reaching the LIA moraines position, thus represented at its maximum advance during
that period and; (F) presentPresent-day situation characterized by the MPG divided
into two ice bodies, no ice remaining from the LIA, and very steep slopes (sampling
transect indicated by a red line).

902 **Table 1.** Concentrations of ^{137}Cs in the soluble water fraction of ice from Monte
903 Perdido samples. [MDA: Minimum Detection Activity](#)

Sample	Mass of ice analyzed (g)	^{137}Cs activity ($\text{Bq}\cdot\text{L}^{-1}$)	MDA ($\text{Bq}\cdot\text{L}^{-1}$)
MP-61	240	< MDA	0.15
MP-82	178	< MDA	0.16
MP-97	232	< MDA	0.14
MP-98	376	< MDA	0.09
MP-100	238	< MDA	0.17

904

905

906 **Table 2.** Determination of ^{210}Pb activity in the soluble water fraction of 100 g of ice
907 from Monte Perdido samples. [MDA: Minimum Detection Activity](#).

Sample	^{210}Pb activity ($\text{mBq}\cdot\text{L}^{-1}$)	MDA ($\text{mBq}\cdot\text{L}^{-1}$)
MP-73	17.4 ± 2.6	1.14
MP-76	6.2 ± 1.3	0.70
MP-82	<MDA	0.61
MP-85	<MDA	0.84
MP-88	<MDA	1.23
MP-91	<MDA	1.05
MP-94	<MDA	0.71
MP-97	<MDA	0.77
MP-98	<MDA	0.58
MP-100	8.5 ± 1.5	0.71

908

909

Table 3. Radiocarbon dating of MPG samples indicating their origin, the radiocarbon age (^{14}C age BP) and the calibrated date using INTCAL13 curve and presented in calendar years Common Era (CE). Samples in ~~red and~~ *italics* were not included in the depth-age model (see column “comments” and text for explanation).

Sample origin	Sample ID	Laboratory ID	^{14}C age BP	Cal age (CE)	Comments
Bulk organic matter	MP-1	D-AMS 025291	2000±64	8±66	Used in the age model
	MP-42	D-AMS 025294	1554±27	462±32	Used in the age model
	MP-48	D-AMS 025295	73±33	<i>1897±20</i>	<i>Discarded due to plastic contamination</i>
	MP-67	D-AMS 025296	876±29	1185±31	Used in the age model
	MP-68	D-AMS 026592	1128±22	942±24	Used in the age model
	MP-69	D-AMS 026593	1230±23	730±14	Used in the age model
	MP-70	D-AMS 025297	1308±28	680±16	Used in the age model
	MP-73	D-AMS 025298	1011±25	1012±16	Used in the age model
	MP-100	D-AMS 025299	923±39	1074±31	Used in the age model
Bulk material (filter)	MP-67filter	D-AMS 029894	485±40	<i>1429±15</i>	<i>Discarded due to mixing with detrital fraction</i>
	MP-81filter	D-AMS 033972	1758±25	<i>287±68</i>	
WIOC	MP10m	MP10m	812±755	<i>854±721</i>	<i>Discarded due to too high error</i>
	MP59m	MP59m	926±268	1046±242	Used in the age model
Pollen concentration	MP-30pollen	D-AMS 031464	3906±42	<i>-2384±1332</i>	<i>Discarded due to technical issues and too high errors</i>
	MP-70pollen	D-AMS 031465	1787±37	<i>237±255</i>	
	MP-100pollen	D-AMS 031466	1854±30	<i>158±807</i>	

915 **Table 4.** Elemental concentration (ppm) of major and trace metals in both Ordesa's
916 current deposited dust and MPG ice deposits (averaged values for the 35 analyzed
917 samples), as well as Upper Crust (UC) elemental contents for comparison (Taylor and
918 McLennan, 1995). On the right side, Al-normalised Enrichment Factors (EF) for dust
919 components and elements for: EF_i, the MPG ice dust versus the current Ordesa's
920 deposited dust (Codd); EF_{Codd}, the Codd versus the UC; and EF_{IMPGID}, the MPG ice
921 dust versus the UC. Numbers in bold italics type in the EF represent anomalous values
922 (elements enriched in Ordesa samples or in MPG ones).

	Ordesa 2016-2017 (2-year atmospheric deposition)			Monte Perdido (ice dust: 35 filter samples)			Upper Crust (ppm)	Al-Normalised Enrichment Factors		
	Max	Min (ppm)	Average	Max	Min (ppm)	Average		EF _i	EF _{Codd}	EF _{IMPGID}
OC	443270	49659	206814	436343	14793	126381		0.4		
EC	114519	12506	39995	112769	14668	40605		0.6		
Al	122401	7883	60410	506467	19611	98808	80400	1.0	1.0	1.0
Ca	22578	3182	9663	119648	256.7	11984	30000	0.8	0.4	0.3
Fe	63218	2901	32665	183957	12504	59477	35000	1.1	1.2	1.4
K	27478	3907	14839	57038	4001	18505	28000	0.8	0.7	0.5
Mg	27286	2105	12265	72210	3513	16645	13300	0.8	1.2	1.0
Na	5380	1.2	1413	25750	593	5126	28900	2.2	0.1	0.1
Ti	5035	257	2334	52192	3243	13662	3000	3.6	1.0	3.7
Mn	1656	128	582	3835	174	979	600	1.0	1.3	1.3
Sr	170	19	78	200	20	80	350	0.6	0.3	0.2
Be	7	0	2.1	2.3	0	0.4	3	0.1	0.9	0.1
V	208	10	76	257	28	107	60	0.9	1.7	1.5
Cr	720	5	118	2915	12	441	35	2.3	4.5	10.3
Co	32	0	7.6	49	5.4	20	10	1.6	1.0	1.6
Ni	414	7	55	1046	4.3	228	20	2.5	3.6	9.3
Cu	683	33	127	26451	92	3786	25	18.3	6.7	123.2
Zn	9391	164	1316	3826	171	988	71	0.5	24.7	11.3
As	26	2	10	51	5.3	18	1.5	1.0	9.1	9.6
Se	90	0	22	30	0	5.2	50	0.1	0.6	0.1
Cd	100	0	14	1.5	0	0.3	0.98	0.0	18.8	0.2
Sb	26	0	4.5	59	2	11	0.2	1.5	29.7	43.3
Ba	1010	15	287	870	67	317	550	0.7	0.7	0.5
Tl	1	0	0.1	1.1	0	0.2	0.75	1.7	0.1	0.2
Pb	175	8	53	2989	86	495	17	5.7	4.2	23.7
Th	37	1	12	26	1.6	9.7	10.7	0.5	1.5	0.7
U	8	0	2.5	15	0	3.7	2.8	0.9	1.2	1.1

925 [Table 5. Values of Pb/Al ratio and Hg concentration from MPG samples \(plotted in Fig.](#)
926 [4\).](#)

Pb/Al ratio in MPG			Hg in MPG		
Sample ID	Age (yr AD)	Pb/Al	Sample ID	Age (yr AD)	Hg (µg/g)
MP-1	9.7	0.0085	MP-1	9.7	0.00023
MP-4	38.9	0.0024	MP-5	48.6	0.00010
MP-7	68.0	0.0041	MP-10	97.1	0.00017
MP-10	97.1	0.0068	MP-15	145.7	0.00021
MP-13	126.3	0.0059	MP-20	194.3	0.00012
MP-16	155.4	0.0060	MP-25	242.9	0.00037
MP-19	184.6	0.0065	MP-30	291.4	0.00018
MP-22	213.7	0.0098	MP-35	340.0	0.00026
MP-25	242.9	0.0037	MP-40	388.6	0.00019
MP-28	272.0	0.0054	MP-45	437.1	0.00073
MP-31	301.1	0.0064	MP-50	485.7	0.00014
MP-34	330.3	0.0046	MP-55	534.3	0.00009
MP-37	359.4	0.0099	MP-60	582.9	0.00015
MP-40	388.6	0.0064	MP-65	631.4	0.00024
MP-43	417.7	0.0049	MP-70	680.0	0.00024
MP-46	446.9	0.0040	MP-75	1017.3	0.00014
MP-49	476.0	0.0047	MP-80	1053.8	0.00022
MP-52	505.1	0.0054	MP-85	1090.4	0.00019
MP-55	534.3	0.0071	MP-90	1126.9	0.00013
MP-58	563.4	0.0030	MP-95	1163.5	0.00023
MP-61	592.6	0.0041	MP-100	1200.0	0.00021
MP-64	621.7	0.0068			
MP-67	650.9	0.0018			
MP-70	680.0	0.0056			
MP-76	1024.6	0.0026			
MP-79	1046.5	0.0017			
MP-82	1068.5	0.0033			
MP-85	1090.4	0.0038			
MP-88	1112.3	0.0030			
MP-91	1134.2	0.0039			
MP-94	1156.2	0.0044			
MP-97	1178.1	0.0040			
MP-98	1185.4	0.0038			
MP-100	1200.0	0.0013			

927